

# Investigation of the Impact of Non-Uniform Permeability on Axial Gas Transport within Light Water Reactor Fuel Rods during a Loss Of Coolant Accident and Clad Failure

Chiara Genoni<sup>a</sup>

*???*  
come contesto dc,  
*???*  
<sup>a</sup>Idaho National Laboratory, Idaho Falls, ID, U.S. ma le tue analisi sono  
su separate effect

**Abstract** QUESTO ABSTRACT HA TROPPO BLABLA E NON HA I RISULTATI  
NÈ LA METODOLOGIA PER OTENERLI, NÈ DEGLI OBIETTIVI PRECISI

The time-scale of plenum depressurization during a typical LOCA and clad failure in a LWR plays a fundamental role in either favoring or preventing further fuel rod damage. Indeed, if cladding ballooning occurs, the established axial pressure gradient induces flow of gas from the fuel rod plenum through the stack of fragmented pellets. As a result, the ballooned region gradually undergoes pressurization, and if emergency cooling systems are not activated in time, cladding burst becomes a potential outcome. At this stage, depending on the state of fuel fragmentation (which is related to fuel burn-up), small highly radioactive fuel particles could be ejected into the reactor vessel, and the main safety requirement of maintaining a fuel rod coolable geometry cannot be guaranteed. Therefore, with the interest of surpassing the regulatory limits on fuel burn-up while ensuring the fulfillment of all safety standards, modeling and experimental advancements for the investigation of LWR fuel rods axial gas transport phenomenon in accidental scenarios are required. The present work presents a model of the experimental setup assembled at Idaho National Laboratory (INL), employing Computational Fluid Dynamics (CFD) simulation tools provided by the Multi-physics Object Oriented Simulation Environment (MOOSE). The experiment aimed at examining the relationship between the severity of fuel fragmentation and axial gas transport by coupling pressure decay measurements with results of the fragmented pellets image analysis performed through X-ray computed tomography. In the CFD model, the problem is treated as gas flow through a porous medium. The primary focus of this investigation is to examine how the non-uniform permeability, varying along the axial direction, impacts the time-scale of plenum depressurization. More precisely, distinct permeability values are assigned to individual pellets, and simulations are conducted by considering all possible combinations of pellet positions.

**Keywords:** Light Water Reactor, Fuel Fragmentation, Relocation and Dispersal, Loss Of Coolant Accident, Axial Gas Transport

## IN INTRÒ DOVRESTI DARMI TUTTO LO STATO DELL'ARTE CHE MI SERVIRÀ CON LE MOTIVAZIONI

1. Introduction The nuclear industry has always been investing a significant effort at increasing Light Water Reactors (LWRs) average rod discharge burn-up above the regulatory limits, aiming at the improvement of the power plant economic efficiency and the reduction of discharged spent fuel volume. Clearly, many challenges need to be addressed in order to achieve such goal. One crucial aspect is to investigate Fuel Fragmentation, Relocation and Dispersal (FFRD) related phenomena and understand their implications within the regulatory framework.

FFRD can potentially occur during a LOCA if fuel rods are exposed to specific conditions. However, the possibility of fuel fragmentation on its own is not a safety concern, but it may have an impact on regulatory figures of merit if combined with axial relocation and dispersal, both phenomena that are highly influenced by fuel burn-up. Indeed, the consequences of FFRD are unlikely to result in an imminent safety hazard as their magnitude is limited by the regulatory constraints on the discharge fuel burn-up.

In a typical LOCA scenario, the heat removal process is impeded, possibly causing the cladding to experience ballooning. If the cladding radial strain is greater than 3% and the pellet average burn-up is above 55 GWd/t, the resulting small fuel fragments can experience axial relocation in the ballooned region,

with formation of local hot-spots exposed to higher heat loads Pettersson et al. (2009). This event can result in an increase in the cladding deformation extent, thus raising the likelihood of damage. Also, experimental data demonstrated that significant quantities of fission gas may be released during a LOCA transient, and this phenomenon has an impact on the further fuel rod ballooning and burst behavior, increasing importantly with increasing burn-up.

Another factor playing a fundamental role in the development of FFRD is the time for plenum depressurization. The pressure difference that is established between the plenum and the ballooned region induces flow of gas along the axial direction, and depending on the gas flow speed and the time of the ballooning event, it may either prevent or favor further cladding deformation. If the cladding ballooning occurs early in the LOCA and the gas flow is slow, the emergency cooling systems have time to lower the cladding temperature before their correct functioning is impeded by the extent of cladding deformation itself. On the other side, if the gas flow is fast, further pressurization in the ballooned region may lead to channel blockage and potentially to cladding rupture. After cladding burst, still the state of fuel fragmentation remains a major concern. If the size of fuel fragments is smaller than the cladding rupture, highly radioactive material can potentially be ejected

into the primary loop, which violates the requirement of maintaining a coolable fuel geometry.

Clearly, conducting comprehensive experimental and modeling studies on the FFRD phenomenon is crucial. Such advancements hold the potential to yield significant benefits not only from an economic standpoint, but also in the perspective of developing advanced technology fuels, as nuclear fuels in advanced reactors are similarly clad in materials that are designed to contain the fission gases from the release to the primary coolant system. The present work specifically focus on the time for plenum depressurization driven by the axial gas transport phenomenon through the fragmented pellets, and on the investigation how it is influenced by the state of fuel (including gap thickness and severity of cracking), which is related to the burn-up level. By conducting detailed analyses and experiments, valuable insights can be gained to maximize fuel burn-up.

## 2. Theory



Fuel fragmentation can be attributed to two primary causes: the development of a strong radial thermal gradient inside the fuel pellet and the removal of hydrostatic pressure conditions. The former arises during normal operational conditions, inducing pellets fracturing due to the establishment of high internal stresses. In this phase, the number of fuel fragments increases almost linearly with the fuel rod linear power Oguma (1983). Besides, as the burn-up increases throughout the lifetime of fuel inside the reactor core, further cracking attributed to material damage due to irradiation or thermal cycling is observed up to 50 GWd/t Walton and Husser (1983). The latter type of fragmentation occurs during cladding ballooning and its severity depends on the extent of the High Burn-up Structure (HBS). The presence of hydrostatic pressure is a consequence of pellet-gap interaction arising from the combined effects of fuel swelling and cladding creep down. In the ballooned region, the elimination of this interaction results in fuel cracking, whose severity is correlated to the development of the HBS. Similar effects appears even if the gap is open, caused by the abrupt drop in pressure when cladding ballooning and rupture occur Turnbull et al. (2015).

In any case, the size of the resulting fuel fragents is always related to the burn-up level. As part of the Halden Reactor Project, an extensive series of tests was performed on Light Water Reactor (LWR) fuel rods with burn-up levels reaching up to 90 GWd/t, yielding valuable data about the performance of fuel rods during LOCA transients. For some of the LOCA tests, a detailed observations were made on the fragmentation patterns occurring in fuel pellets near the ballooned and burst regions. These investigations led to the identification of three distinct fuel conditions, each dependent on the level of fuel burn-up:

- Cracked: from fresh fuel to approximately 40-50 GWd/t, pellets are fragmented into a countable number of 3-4 mm size pieces.

- Coherently Fragmented: from 40-50 GWd/t to approximately 70-80 GWd/t a reduction of particle size is observed, with a uniform distribution between 0.1 and 4 mm.
- Pulverized: above 70-80 GWd/t, the particle size distribution is characterized by the prevalence of very small fragments and powder in the 0.1-1mm size range. The number of small fragments increases in time. ↗

The observed thresholds align well with the average burn-up limit of the fuel rods coinciding with the onset of the High Burn-up Structure (HBS), which is formed when the local burn-up at the rim exceeds approximately 60 GWd/t (40-45 GWd/t radial averaged). The HBS is characterized by a fine grain structure and high porosity resulting from the accumulation of fission gas bubbles Bianco et al. (2015). The phenomenon of pulverization occurs within the HBS, while fuel fragmentation leading to larger particle sizes is located outside this region. With increasing burn-up, the extension of the HBS expands, intensifying the pulverization process.

Many experiments performed in the past were able to demonstrate that axial gas transport phenomenon inside fuel rods is somehow influenced by the severity of fuel cracking, including the ones at the Organisation for Economic Cooperation and Development (OECD) Halden Reactor Project, Oak Ridge National Laboratory (ORNL), INL and at the Joint Research Centre in Germany. The experimental approaches that were adopted consisted in following one of the two methodologies Čalogović (1995):

- Producing a uniform pressure different from the surrounding inside the fuel rod, open a valve at the outlet to establish a pressure difference, and then measure the plenum pressure decay due to the flow of gas through the fuel stack (Transient Test).
- Imposing a constant gas flow rate and measuring the rod pressure difference between transducers positioned at various positions along the axial direction (Steady State Test).

Still as part of the Halden Reactor Project, two essential in-pile experimental series, known as IFA-430 and IFA-504, were conducted focusing on measuring gas flow resistance in terms of hydraulic diameter. During these experiments, eight fuel rods were loaded into the Halden Reactor, and the hydraulic diameter was continuously monitored. Starting from the initial period of irradiation, such measurements were taken as the power was increased until the assembly was eventually discharged (at 22.5 GWd/t for IFA-430 and 60 GWd/t for IFA-504). During the initial stages of the experiment, the hydraulic diameter of the fuel rods coincided with the manufactured gap thickness. However, as the power ramped up, fuel pellets fragmentation initiated, leading to a decrease in hydraulic diameter. Subsequently, further reduction was caused by fuel swelling at a rate of 1% per 10 GWd/t, until almost approaching a constant value Turnbull (1995).

At ORNL, researchers conducted measurements of permeability on eight full-length Pressurized Water Reactor (PWR) rods, characterized by a burn-up ranging from 48 to 59 GWd/t.

The resistance to flow was found to exhibit a clear dependence on the fuel burn-up, displaying an increasing trend. Also, it resulted to be influenced by the pressure gradient established along the fuel rod Montgomery and Morris (2019).

Another important experiment to be mentioned is the one performed at the JRC in Germany, where nitrogen gas permeability measurements through a spent LWR fuel rod were performed at room temperature, applying several pressure levels. The fuel rod had a average burn-up of 52 GWd/t. The experiment was able to demonstrate a reduction in the time for plenum depressurization with increasing pressure difference established across the fuel rod Y et al. (2015).

However, none of the two previously mentioned experiments was supported by a detailed fuel pellets image analysis. In all cases, a dependency of the resistance to flow on the state of fuel fragmentation was observed, but they were never focusing in finding the relationship on morphological features of fuel cracking.

*DA QUI, NON SEMBRA "THEORY" ...*

The only experimental activity provided of metallography image analysis was conducted by INL. Axial gas flow experiments were performed on six full-length fuel rods, removed from an PWR assembly with an average and peak burn-up of 28 and 31 GWd/t, respectively. The measurements were conducted at ambient temperature and at 533K, using both helium and argon as filling gas. One fuel rod was sectioned in 8 portions, and metallographic measurements of the average gap and crack thickness were made. The experiment was able to demonstrate that the hydraulic diameter, measured through gas flow experiments, was consistently different than the effective gap size measured through metallography (radial gap + cracks). Such deviation was always observed to be negative, due to the additional friction produced by the extremely tortuous paths Dagbjartsson et al. (1977).

To reduce the uncertainty in the fuel rod gas flow resistance, a correction factor needs to be added, embedding the dependency upon parameters describing morphological features of fuel fragmentation. The separate-effects experiment that is simulated in the present work uses non-irradiated fuel specimens, exposed to mechanical and thermal loads to mimic different states of fuel irradiation. Each pellet is exposed to X-ray computed tomography, and the 3D porosity distribution is assessed using MATLAB. The ultimate goal is to derive such correction factor in the resistance to flow that accounts for the effect of gas flowing through the cracks.

(here I have to add state-of-the-art from the modeling side)

- Analytical Methodology applying Hagen-Poiseuille's or Darcy's law Vincenzo et al. (2015), Dagbjartsson et al. (1977).
- numerical computation of permeability in a cracked spent fuel, using finite element method to solve gas flow and a 3D mesh of crack networks Thomas et al. (2018).

### 3. Materials and Methodology

#### 3.1. Experimental Set-Up

The experimental set-up consists of stainless steel rods containing from four to eight fragmented alumina pellets that were previously exposed either to mechanical or thermal loads to mimic different states of fuel damage. In Tab.1 are listed the geometrical parameters. In some cases the whole pellets stack is wrapped in a Mylar foil (2-4 mil thickness), whereas in others each pellet is singularly wrapped. Wrapping is required to preserve the pellets cylindrical shape, but also to allow the gap filling with silicon rubber or epoxy resin. The latter procedure is fundamental to mimic the case when the gap is closed.

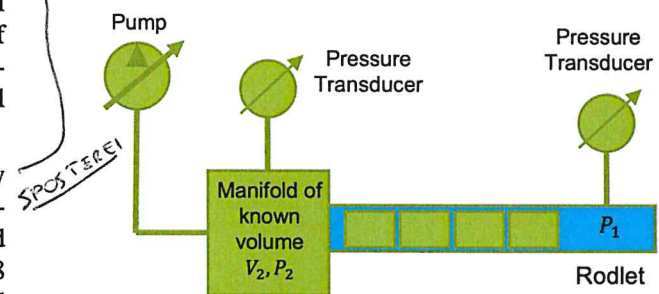


Figure 1: Schematic representation of experimental setup.

Pellets Radius	7.94 mm
Pellets Height	7.94 mm
Cladding Radius	8.24 mm
Cladding Length	152 mm

Table 1: Geometrical parameters of the experimental set-up.

The rod is pressurized adiabatically by pumping air at environmental temperature, until approaching a condition of uniform pressure. A quick-acting valve located at one side of the rod is opened, and the pressure decay is measured on both sides through transducers (inlet and outlet). The time for plenum depressurization is expected to vary depending on the severity of cracking in the alumina surrogates. The measurement of the pressure decay was performed twice for each level of pressurization (600, 800 and 1000 psi). Experimental data were collected for tubes with different number of pellets at different states of fragmentation, and with either the gap open or closed.

#### 3.2. Image Analysis

Here I have to ask Tommaso to give me a summary of what he has been doing + pictures/plots

UPDATES?

#### 3.3. Modeling

In the present work, Computational Fluid Dynamics simulation tools provided by the Multiphysics Object Oriented Simulation Environment (MOOSE) are employed to simulate the experimental set-up. MOOSE is a parallel finite element framework developed at INL that provides a robust infrastructure for

solving coupled systems of partial differential equations. It is also provided of finite volume tools for modeling and analyzing a wide range of physical phenomena involving fluid flow, heat transfer, and other multi-physics processes Gaston et al. (2009).

The CFD model is created in support of experimental activities, offering the opportunity to capture more physics and to describe a more complex system beyond the limitations of simply applying the solution of Darcy's equation (Eq.1).

$$\frac{P_{in}(t) - P_{out}}{P_{in}(t) + P_{out}} = \frac{P_{in}(0) - P_{out}}{P_{in}(0) + P_{out}} e^{-\frac{KA}{\mu L V} t} \quad (1)$$

where  $A(m^2)$  is the fuel stack cross sectional area,  $V(m^3)$  is the plenum volume,  $L (m)$  is the pipe length,  $P_{out}(Pa)$  and  $P_{in}(Pa)$  are the pressure at the outlet and the inlet, and  $\eta(Pa \cdot s)$  is the fluid viscosity.  $K(m^2)$  is the permeability factor, representing the ability of a medium to allow fluid to pass through its porous structure. In a fuel rod,  $K$  depends on the condition of pellet-cladding gap and the severity of fuel cracking, both of them expected to be varying spatially along the axial direction. Indeed, by the end of the first fuel cycle (25 GWd/t) in some portions of the fuel rod the gap completely closes due to the combined effect of fuel swelling and cladding creep down, while the upper and lower portions of the fuel rod may still exhibit a discernible gap due to the non-uniform flux distribution along the axial direction.

The main limit of applying the analytical methodology is the impossibility of considering such non-uniformities. On the other side, in the CFD model Navier-Stokes equations can be solved accounting for spatial and time dependent material properties or boundary conditions. Also, it permits to change and easily manipulate parameters such as fuel rod length and diameter, temperature, type of filling gas and permeability. Such parametric study can be easily performed using the Stochastic Tools Module in MOOSE, that allows to vary a set of input parameters and computing quantities of interest. The module is capable of running multiple simulations at the same time, and if coupled with the High Performance Computing resources provided by INL has the potential of drastically reduce the computation time.

For the purpose of this specific study, the CFD model was indispensable. The reason lies in the impracticability of the experiment, as the permutation of pellet positions would necessitate the extraction of all fragmented pellets from the fuel rod, resulting in their disintegration, and the subsequent reassembling of the pellets would be almost impossible. The proposed approach involves assigning a distinct permeability value to each fuel pellet and conducting simulations for all possible configurations to predict plenum depressurization. In each configuration, the positions of the pellets will be varied.

The CFD model will be validated by fitting the predicted plenum pressure decay with the experimental data, aiming at finding some correlation between permeability factor and morphological features of the porous structure, including porosity, tortuosity and pellets specific surface. The estimation of such parameters is performed using Dragonfly Software, by inputting the results of a segmentation procedure applied to cross

section images of each fuel pellets taken though X-ray computing tomography. The resulting formula is used to select some reasonable parameters of permeability to be used to perform the study regarding the effect of considering a non-uniform permeability on the time for plenum depressurization.

### 3.4. CFD Model Description

The fuel stack is modeled as single domain with uniform properties, implying no distinction between the gap and the fragmented pellets. A two-dimensional axial-symmetric mesh was used with 300 and 5 elements in the axial and radial direction, respectively. A crucial matter in this type of fluid dynamics problems in which gas flow is driven by an extremely high pressure difference is to determine if fluid flow can be considered compressible or not. The difference between the two flow regimes is conceptually simple: a compressible fluid can experience a change in density during the flow while an incompressible does not experience such change. Although all fluids are potentially compressible, usually liquids are considered incompressible, but this assumption cannot be stated a priori for a gas. A general criterion consists in evaluating the Mach number, defined as the ratio between the fluid velocity and the speed of sound. If the Mach number is lower than 0.3, the gas compressibility is negligible. MOOSE includes both compressible and incompressible flow models, but the finite time-scale of plenum depressurization suggested to start by using the Weakly-Compressible Navier-Stokes (WCNS) equations (Eq.2), and eventually estimate the fluid velocity to guarantee the flow not to be in a compressible regime.

$$\begin{aligned} \frac{\partial \rho}{\partial t} + \nabla \cdot (\rho \vec{u}) &= 0 \\ \frac{\partial(\rho \vec{u})}{\partial t} + \nabla \cdot (\rho \vec{u} \times \vec{u}) - \nabla \cdot (\mu \nabla \vec{u}) + \nabla P &= -F_1 \vec{u} - F_2 |\vec{u}| \vec{u} \end{aligned} \quad (2)$$

where  $\vec{u}$  is the fluid velocity,  $P$  is pressure,  $\rho$  is density and  $\mu$  is the dynamic viscosity. The additional density time-derivative in the continuity equation and the coupling of the ideal gas law allows to account for gas compressibility without any need of adding terms that describe the propagation of acoustic waves, which is typical of a fully compressible flow regime. A uniform pressure of 4.3 MPa is imposed inside the tube as initial condition, as well as a uniform porosity distribution given by the gap volume fraction. Time-varying outlet boundary conditions are imposed and no slip wall boundary conditions are also assumed.

$F_1 = \mu/K_1$  is the Darcy friction factor, used to account for viscous losses in laminar flow regime.  $F_2 = \rho/K_2$  is the Forchheimer friction factor, commonly added in porous flow NS equations to account for inertial forces arising in turbulent regime ( $Re > 10$ ). In this specific system, the assumption of turbulent regime is made a priori due to the high pressure gradient that is established along the fuel rod, and  $Re$  will be evaluated afterwards.

$K_1$  and  $K_2$  can be estimated using Ergun equations:

$$K_1 = C_1 \frac{\epsilon^3}{(1-\epsilon)^2} \quad (3)$$

7 4  
MESCOLI  
TROPO

QUESTO È IL CONTRARIO  
DI VALIDAZIONE

$$K_2 = C_2 \frac{\epsilon^3}{(1-\epsilon)} \quad (4)$$

Eq.3 and 4 two are semi-empirical formulas originally intended to be used for isotropic granular porous media consisting of spherical particles at medium porosity. Both of them could be extended to other porous structures, although potentially involving high uncertainty. For this reason, much effort has always been invested in the development of corrections to improve the prediction of permeability for different types of porous materials Zhu (2023).  $C_1$  and  $C_2$  are factors than requires to be empirically determined, containing the dependencies upon morphological features of the porous structure.  $\epsilon$  is the porosity, which is given by the sum of two contributions (see Eq.5): one associated to the gap and the other associated to the pellets. The former is defined as the ratio between the gap and the total fuel rod cross sectional area, whereas the latter is estimated through image analysis (MATLAB, ecc). Such approach consists in smearing out the porosity across the entire domain, with no distinction between gap and fragmented pellets.

$$P_{\text{smeared}} = \frac{D_{\text{clad}}^2 - D_{\text{fuel}}^2}{D_{\text{clad}}^2} + P_{\text{fuel}} \cdot \frac{D_{\text{fuel}}^2}{D_{\text{clad}}^2} \quad (5)$$

BANALOTIA

#### 4. Results

##### 4.1. CFD Model Validation

Validation of the CFD model is performed considering six sets of experimental data. Specifications of all experiments are listed in Tab.2. Porosity is estimated using Eq.5, considering also the presence of the Mylar wrapping, whose effect is to reduce the gap thickness of  $75 \mu\text{m}$ .

On TT1 experiment series, in a first attempt of model validation, the Forchheimer friction factor contained in NS equations was neglected. However the predicted pressure decay showed important deviations from the experimental results, growing bigger as the initial pressure level was increased. An estimation of the Reynolds number distribution along the axial direction was performed, and resulted to be increasing as approaching towards the outlet. Maximum Reynolds numbers of 40, 33 and 24 are reached at  $t = 0\text{s}$  (listed in order of increasing initial pressure), tending to decrease throughout the simulation, allowing a transition from turbulent to laminar flow regime. These results are clear evidence that the Forchheimer friction factor must be included in the NS, given that the flow regime is mainly turbulent. By fitting the predicted pressure decay on the experimental data, it is possible to estimate  $K_1$  and  $K_2$ . In Fig.3 is shown a comparison of the plenum pressure decay computed including and excluding the Forchheimer friction factor, respectively. If turbulence is neglected, important negative deviations from the experimental data appears at the beginning of the decay, which is where the Forchheimer friction factor has the most effect as it is quadratically dependent on the gas velocity.

Similar behavior are expected also for CT1 and CT2 experiment series (still need to validate these experiments).....

Name	TT1	CT4	CT1	CT2
Tube ID (mm)	8.24	8.24	8.24	8.24
Pellet OD (mm)	7.94	7.98	7.94	7.94
Pellet Status	crushed	quenched	fresh	quenched
Gap Status	open	filled	open	open
Gap Thickness ( $\mu\text{m}$ )	150	110	150	150
Gap Porosity (%)	3.6	2.6	3.6	3.6
Fuel Porosity (%)	2.0	1.5		

Table 2: Specifications of experiment series.

On the other side, in CT4 experiment series, good predictions of the experimental results are obtained even though the Forchheimer friction factor is neglected. The reason of this behavior can be attributed to significantly higher resistance to flow that maintains the flow predominantly laminar regime for most of the simulation. The factors contributing to the higher resistance: the smaller manufactured gap thickness, the presence of epoxy resin in the attempt of completely closing the gap, and possibly the state of fuel fragmentation.

In Tab.3 are reported the best-fit permeability values for TT1 and CT4. In Fig.5 are plotted such values of permeability (only  $K$  for now, but it must be performed with  $K_1$  and  $K_2$  as well) against the smeared porosity, at different initial pressure levels. Eq.3 is fitted on the experimental data to estimate the empirical factor  $C_1$ , that resulted to be equal to  $2.3\text{e-}10$ ,  $9.6\text{e-}11$ ,  $6.6\text{e-}11 \text{ m}^2$ , listed in order of increasing intial pressure.

Pressure (MPa)	4.3	5.6	7.0
$K_1(\text{m}^2)$	-	-	-
$K_2(\text{m/kg})$	-	-	-
$K(\text{m}^2)$	$2.9 \cdot 10^{-15}$	$1.8 \cdot 10^{-15}$	$1.8 \cdot 10^{-15}$

Pressure (MPa)	4.3	5.6	7.0
$K_1(\text{m}^2)$	$7.4 \cdot 10^{-13}$	$6.6 \cdot 10^{-12}$	$3.3 \cdot 10^{-13}$
$K_2(\text{m/kg})$	$3.1 \cdot 10^{-10}$	$2.5 \cdot 10^{-10}$	$2.5 \cdot 10^{-10}$
$K(\text{m}^2)$	$2.9 \cdot 10^{-15}$	$2.0 \cdot 10^{-14}$	$1.3 \cdot 10^{-14}$

Table 3: Permeability coefficients at different pressure levels.

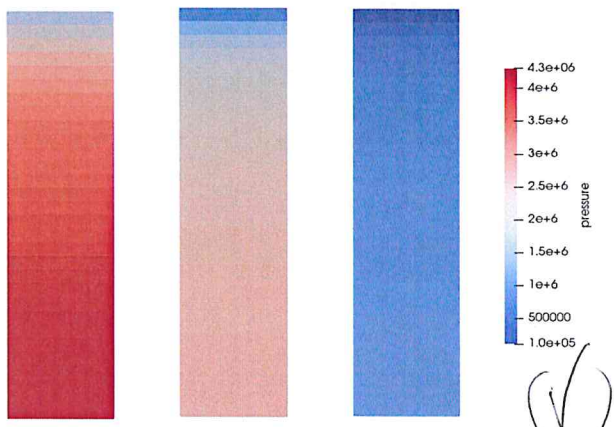


Figure 2: Snapshots of CFD simulation of CT4 at 2s, 10s and 40s, with initial pressure of 4.3 MPa.

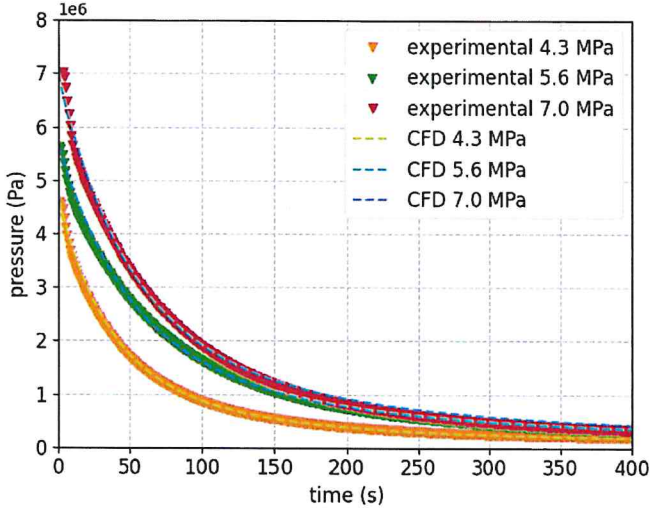


Figure 4: Best-fit curves excluding the Forchheimer coefficient for experiment CT4, at different pressure levels.

#### 4.2. Sensitivity Analysis

To perform the study regarding the influence of considering non-uniform permeability along the axial direction, proper values of  $K_1$  and  $K_2$  has to be selected and assigned to each single pellet. In order to do that, sensitivity analysis to investigate how porosity influence the time for plenum depressurization requires to be performed. The goal is to find a range of porosity (thus of  $K_1$  and  $K_2$ ) that results in high sensitivity, but making sure that the pressure decay takes a reasonably short time, especially in the perspective of running multiple of them for each possible combination of pellets position, it is important to make sure that the pressure decay does not take too long.

Qui in realta' possiamo anche seguire un altro approccio, che consisterebbe nel calcolare il 4 valori di K dalle porosita' che mi calcola Tommaso per ciascun singolo pellet contenuto all'interno di un fuel rod.

#### 4.3. Pellets Permutation

#### 5. Discussion

#### 6. Future Developments

#### References

- Bianco, A., Vitanza, C., Seidl, M., Wensauer, A., Faber, W., Macián-Juan, R., 2015. Experimental investigation on the causes for pellet fragmentation under loca conditions. *Journal of Nuclear Materials* 465, 260–267. doi:<https://doi.org/10.1016/j.jnucmat.2015.05.035>.
- Čalogović, V., 1995. Gas permeability measurement of porous materials (concrete) by time-variable pressure difference method. *Cement and Concrete Research* 25, 1054–1062. doi:[https://doi.org/10.1016/0008-8846\(95\)00100-Q](https://doi.org/10.1016/0008-8846(95)00100-Q).
- Dagbjartsson, S.J., Murdock, B.A., Owen, D.E., MacDonald, P.E., 1977. Axial gas flow in irradiated PWR fuel rods. Technical Report TREE-NUREG-1158. Idaho National Engineering Laboratory. doi:[10.2172/7283992](https://doi.org/10.2172/7283992).

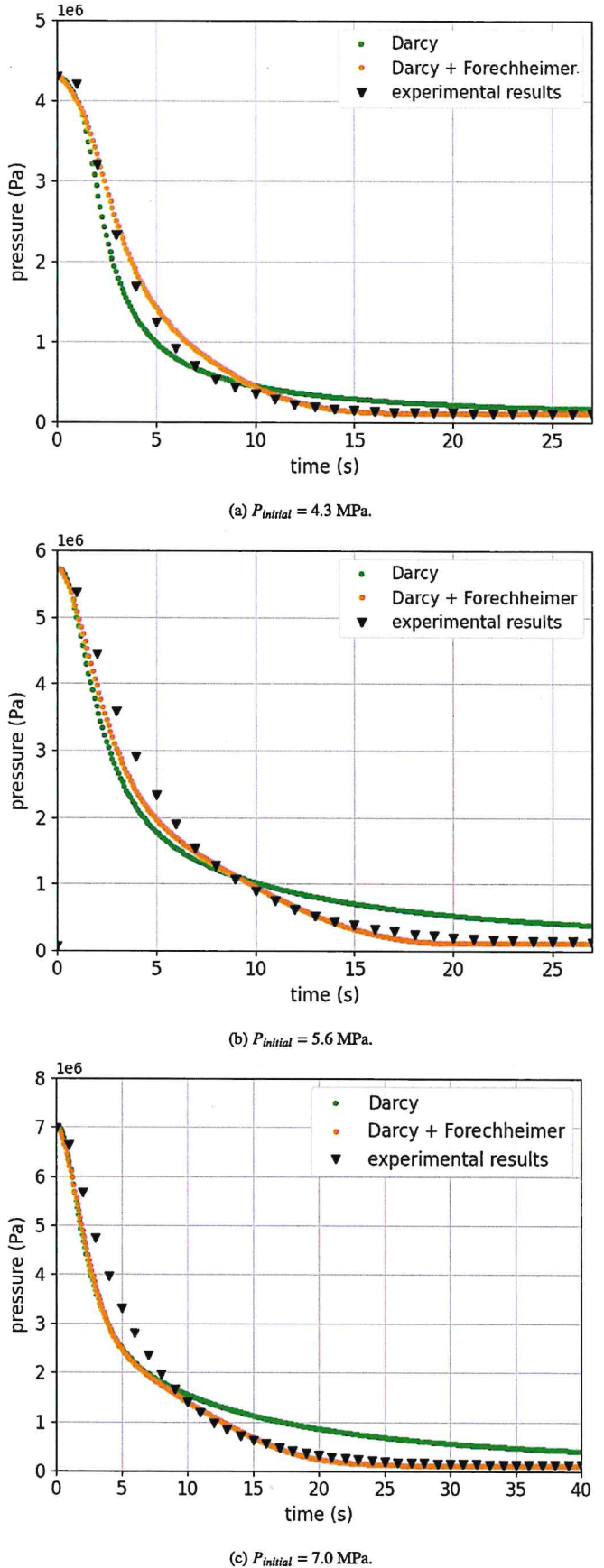


Figure 3: Best-fit curves including and excluding the Forchheimer coefficient for experiment TT1, at different pressure levels.

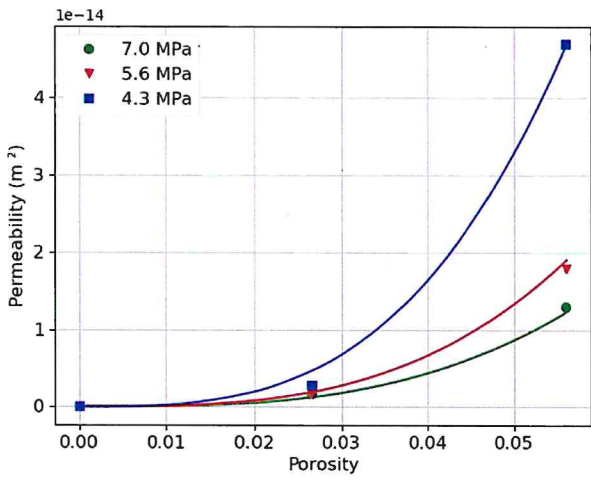


Figure 5:  $K$  as a function of smeared porosity at different pressure levels.

- Gaston, D., Newman, C., Hansen, G., Lebrun-Grandié, D., 2009. Moose: A parallel computational framework for coupled systems of nonlinear equations. Nuclear Engineering and Design 239, 1768–1778. doi:<https://doi.org/10.1016/j.nucengdes.2009.05.021>.
- Montgomery, R., Morris, R.N., 2019. Measurement and modeling of the gas permeability of high burnup pressurized water reactor fuel rods. Journal of Nuclear Materials 523. doi:[10.1016/j.jnucmat.2019.05.041](https://doi.org/10.1016/j.jnucmat.2019.05.041).
- Oguma, M., 1983. Cracking and relocation behavior of nuclear fuel pellets during rise to power. Nuclear Engineering and Design 76, 35–45. doi:[https://doi.org/10.1016/0029-5493\(83\)90045-6](https://doi.org/10.1016/0029-5493(83)90045-6).
- Pettersson, K., Billone, M., Fuketa, T., Grandjean, C., Hache, G., Heins, L., Hózér, Z., Betou, J., Kelppe, S., Mayer, R., Nagase, F., Papin, J., Scott, H., Sonnenburg, H., Sunder, S., Valach, M., Voglewede, J., Vrtílkova, V., Waecckel, N., Zimmermann, M., 2009. “nuclear fuel behaviour in loss-of-coolant accident (loca) conditions.state-of-the-art report”.
- Thomas, R., Paluszny, A., Hambley, D., Hawthorne, F., Zimmerman, R., 2018. Permeability of observed three dimensional fracture networks in spent fuel pins. Journal of Nuclear Materials 510. doi:[10.1016/j.jnucmat.2018.08.034](https://doi.org/10.1016/j.jnucmat.2018.08.034).
- Turnbull, J., 1995. Measuremnt of axial gas trnasport in the gas flow rigs IFA-430 and IFA-504OF. Technical Report. Organisation for Economic Co-operation and Development.
- Turnbull, J.A., Yagnik, S.K., Hirai, M., Staicu, D.M., Walker, C.T., 2015. An assessment of the fuel pulverization thresh- old during loca-type temperature transients. Nuclear Science and Engineering 179, 477–485. doi:[10.13182/NSE14-20](https://arxiv.org/abs/13182/NSE14-20), arXiv:<https://arxiv.org/abs/13182/NSE14-20>.
- V, R., D, P, R, N, W, G, M, R., 2015. Measurement of gas permeability along the axis of a spent fuel rod. European Nuclear Society.
- Vincenzo, R., Dimitrios, P., Ramil, N., Wolfgang, G., Rehm, M., 2015. Mea- surement of gas permeability along the axis of a spent fuel rod, in: Proceed- ings of TopFuel 2015.
- Walton, L.A., Husser, D.L., 1983. Fuel pellet fracture and relocation.
- Zhu, J., 2023. Uncertainty of kozeny–carman permeability model for fractal heterogeneous porous media. Hydrology 10, 21. doi:[10.3390/hydrology10010021](https://doi.org/10.3390/hydrology10010021).